euronoise

Light interaction with leaky acoustic wave radiation in YX-LiTaO3

Paulius Kazdailis, Romualdas Rimeika and Daumantas Ciplys

Vilnius Univ., Dept. of Radiophysics, Saulëtekio al. 9, LT-10222 Vilnius, Lithuania
paulius.kazdailis@ff.vu.lt

The theoretical model and experimental studies of the 633 nm laser light interaction with radiation from leaky surface acoustic waves (LSAW) at various frequencies in YX-lithium tantalate ($LiTaO_3$) are presented. The acousto-optic diffraction with polarization rotation has been observed. The values of bulk acoustic wave (BAW) propagation angle and of the corresponding velocity have been calculated and compared to the ones extracted from the experiment. Differences of the light diffraction process in YX-$LiTaO_3$ from that in ZX-lithium niobate ($LiNbO_3$) have been pointed out. The potential of the described acousto-optic interaction for applications in light control devices and acoustic wave probing has been demonstrated.

1 Introduction

The acousto-optic technique provides flexibility, versatility, and precision to the probing of acoustic wave properties. This makes it very useful for the development and implementation of various acoustic wave-based devices. There is much interest in excitation of bulk acoustic waves (BAW) by interdigital transducers (IDTs), which fit well the standard technologies of electronics industry. YX-lithium tantalate ($LiTaO_3$) has a potential for such applications, since it supports the leaky surface acoustic wave (LSAW) mode with a strong energy radiation into the crystal bulk. The studies of the light diffraction by LSAW-radiated bulk waves deserve much interest because of applicability of their results for both the fundamental investigations and practical applications. The acousto-optic diffraction by the LSAW radiation in ZX-lithium niobate ($LiNbO_3$) has been described in our recent works [1, 2]. In this paper, we report on the light interaction with bulk acoustic waves excited by an IDT at the LSAW resonance in YX- $LiTaO_3$.

2 Experimental setup

The single-crystal $LiTaO_3$ plates of dimensions 15x10x1.5 mm^3 along the crystallographic axes X, Z, and Y, respectively, were used in our experiments. The Y-surfaces of the crystals were flat and parallel optical-grade polished. An IDT for the surface acoustic wave excitation along the X-axis was deposited on the top Y-surface using the standard photolithography. The IDTs with periods of 32 μm, 40 μm, 50 μm, 60 μm, and 120 μm were used. Their electrode pair numbers varying from 15 to 35 are given in Table 1. The aperture of all the IDTs was 1.3 mm. The bottom Y-surface of the crystal was metallized with copper for better light reflection. The refraction indexes of lithium tantalate are n_o=2.175 and n_e=2.18 [3] for the ordinary and extraordinary 633 nm wavelength He-Ne laser light, respectively.

The experimental setup used for the acousto-optic diffraction measurements is schematically shown in Fig. 1. The generator pulses of approximately 1 μs duration modulate the oscillator, which generates the RF pulses of the same duration in the frequency range from 30 MHz to 130 MHz. The RF oscillator output is connected to the IDT and its frequency is tuned to excite the LSAW. The frequency meter is connected to the output of the RF generator. The sample was placed on the rotary stage of the goniometer for a precise variation of the light incidence angle. The rotary axis of the goniometer was in the plane of sample Y-surface, on which the acoustic waves were excited. The light of 633 nm wavelength from the He-Ne laser (*JDSU*) was directed to the point on this axis at the distance of a few millimeters from the IDT. The light was reflected both from the top and the bottom sample surfaces, and the diffracted light was received, through a small diaphragm, by the photomultiplier tube (*HAMAMATSU*). The latter was placed on the goniometer arm, which could be rotated independently from the stage, allowing for an angular selectivity in the light reception. When the RF oscillator frequency was tuned to the leaky wave excitation frequency, the acousto-optic diffraction signal was observed at specific values of the light incidence angle. The polarization of diffracted light was determined with the help of polarizer. The sample and the optical system were so aligned that the axis crossing the center of PMT diaphragm, the incident and diffracted laser beams were in the plane normal to the rotary axis of the goniometer stage and, consequently, to the crystal Y-surface.

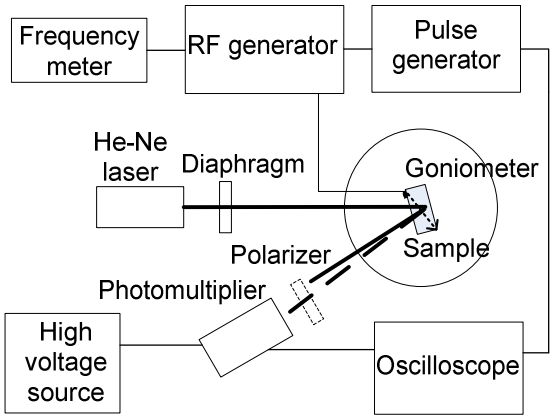

Fig. 1. Scheme of experimental setup.

3 Acoustic wave propagation in YX-$LiTaO_3$

Since an YX-$LiTaO_3$ substrate supports the LSAW mode, the bulk waves in the crystal can be excited with the help of an IDT driven at the leaky wave synchronism frequency. The LSAW synchronism frequencies f_0 were evaluated from IDT impedance measurements with the network analyzer (*AGILENT*), and the LSAW velocity V_L was extracted from these measurements using the relation $V_L = \Lambda f_0$. These f_0 and V_L values for IDTs of different periods Λ are given in Table 1. An average value of the measured LSAW velocity is 3965 m/s. This value differs by less than 2 % from the value 4040 m/s calculated in [4]. The slight deviations from the average of values measured for particular IDTs in our experiment do not exceed 1.5% and can be attributed to the variations in metallisation ratio

and metal film thickness. The LSAW propagating on the crystal surface along the X-direction is strongly damped because of high energy radiation into the sample bulk in the form of BAW [5, 6]. The bulk wave propagation angle α with respect to the crystal surface can be found from the phase matching condition for the leaky and bulk waves:

$$V_L \cos(\alpha) = V_B(\alpha), \quad (1)$$

where V_L and V_B (α) are the LSAW and direction-dependent BAW velocities, respectively. The graphical evaluation of BAW propagation angle (in accordance with Eq. 1) is depicted in Fig. 2. Curves $V_L\cos\alpha$ correspond to our experimental LSAW values obtained for different IDTs and that taken from [4]. The velocity $V_B(\alpha)$ of the slow shear bulk wave was calculated by digitally solving the Christoffel equation with *MATLAB* software. The lithium tantalate material parameters used in calculations were taken from Ref. 7. The fast shear and longitudinal bulk waves are not radiated by LSAW in YX-$LiTaO_3$, since the phase matching condition (1) is not satisfied.

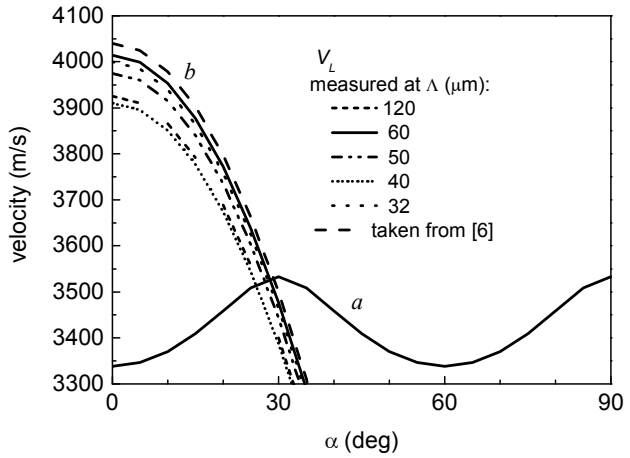

Fig. 2. Velocity of bulk acoustic waves V_B as a function of propagation angle α (curve a) and the product $V_L\cos\alpha$ (curves b).

IDT		1	2	3	4	5
Λ (μm)		120	60	50	40	32
N		15	15	35	20	15
f_0 (MHz)		32.7	66.9	79.5	97.8	124.9
V_L (m/s)	Meas.	3925	4014	3975	3910	4000
	Ref. 4	4040				
α (deg)	From Eq. 1	26.4^0	28.5^0	27.6^0	26.0^0	28.2^0
	Ref. 4.	29^0				
V_B (m/s)	Calc.	3515	3527	3522	3513	3525

Table 1. Acoustic wave velocity and propagation angle values for various IDTs

The bulk wave propagation angle corresponding to the measured average LSAW velocity 3965 m/s is 27.5° and the deviations do not exceed 1.5° (about 5 %). The V_L value of Ref. 4 implies the propagation angle of 29°.

4 Anisotropic acousto-optic diffraction

The wave vector diagram for analysis of interaction of optical and acoustic waves is shown in Fig. 3. It is based on the phase matching condition:

$$\boldsymbol{k_d} = \boldsymbol{k_i} \pm \boldsymbol{K_a}, \quad (2)$$

where $\boldsymbol{k_i}$ and $\boldsymbol{k_d}$ are the wave vectors of incident and diffracted light in the crystal, respectively, and $\boldsymbol{K_a}$ is the acoustic wave vector.

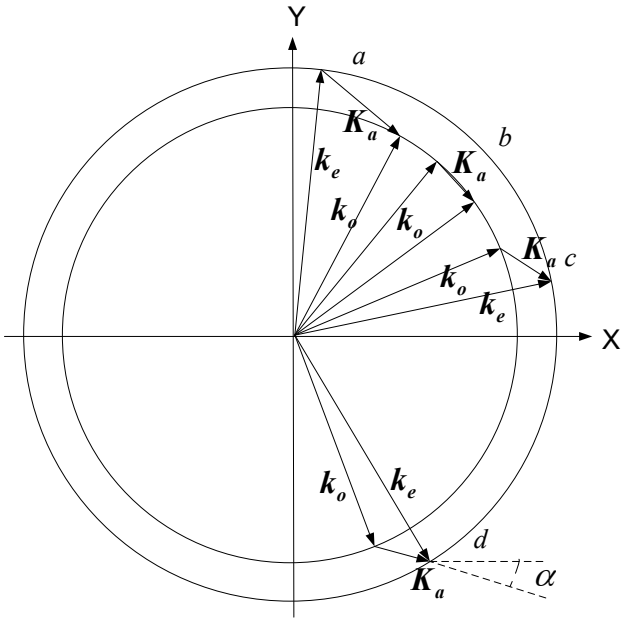

Fig. 3. Acousto-optic diffraction wave vector diagram.

For a given direction of the acoustic wave propagation, there are several wave vector configurations allowed. They are shown in Fig. 3, where the wave vectors of ordinary and extraordinary polarization are marked as $\boldsymbol{k_o}$ and $\boldsymbol{k_e}$, respectively. In the case of an ordinary polarization of the incident light, the "+"sign in Eq. 2 refers to the wave vector configurations *c* and *d* and the "-" sign refers to the configurations *a* and *b*. The latter corresponds to the isotropic diffraction. The configurations *a, c* and *d* correspond to the anisotropic acousto-optic diffraction with the polarization rotation. Cases *b* and *c* were not observed in our experiment because of restrictions arising from the internal light reflection in the crystal.

For a given propagation direction, velocity, and frequency of acoustic waves, the anisotropic acousto-optic diffraction takes place at specific light incidence and diffraction angles, which satisfy the phase matching condition (Eq. 2). The latter can be expressed in the form:

$$n_o \sin\phi_o \pm \frac{f\lambda_0}{V_B(\alpha)}\cos\alpha = n_e \sin\phi_e, \quad (3)$$

$$n_o \cos\phi_o + \frac{f\lambda_0}{V_B(\alpha)}\sin\alpha = n_e \cos\phi_e, \quad (4)$$

where λ_0 is the free-space optical wavelength, ϕ_o and ϕ_e respectively are the direction angles of incident and diffracted wave vectors $\boldsymbol{k_o}$ and $\boldsymbol{k_e}$ (with respect to the crystal Y axis), n_o and n_e respectively are the ordinary and extraordinary refractive indexes of $LiTaO_3$ crystal, α is the direction angle of acoustic wave vector (with respect to the crystal X axis), and $V_B(\alpha)$ is the velocity of BAW propagating at this angle. The "-" sign in Eq. 3 refers to wave vector diagram configuration *a*, while the "+" sign refers to the configurations *c* and *d*. In the case *c* (which was not experimentally studied), the "-" sign should be used in Eq. 4 instead of the "+" sign. By solving the system (3,4), the angles ϕ_o and ϕ_e can be found. The corresponding light propagation angles outside the crystal are evaluated by applying the Snell's law to the light refraction at the crystal surface.

In the experiment, we were able to observe the anisotropic acousto-optic interaction corresponding to the wave vector configurations *a* and *d* shown in Fig. 3. The relevant propagation paths of the interacting waves are depicted in Fig. 4. As shown in Fig. 4*a*, the obliquely propagating acoustic wave interacts with the ordinary light wave reflected from the bottom surface of the sample. The diffracted light beam has an extraordinary polarization and its angle with the surface normal is smaller than that of the incident and reflected beams. This case corresponds to the wave vector configuration *a* of Fig. 3. In the case shown in Fig. 4*b*, the acoustic wave interacts with the ordinary light propagating down from the sample top surface, and the diffracted beam with the extraordinary polarization is reflected from the bottom surface. In contrast to the former case, the diffracted beam makes an angle with the surface normal larger than the light incidence and reflection angle. We were not able to observe the anisotropic diffraction at the configuration *c* of Fig. 3 as well the isotropic diffraction (*b* in Fig. 3) because the diffracted beam was subjected to the total internal reflection at the crystal-air interface.

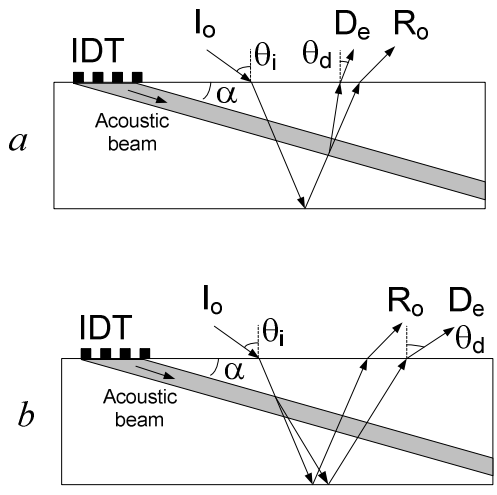

Fig. 4. Light and acoustic wave propagation in the sample (I – incident, R – reflected, D – diffracted beam, $\theta_{i,d}$ – light incidence and diffraction angles, respectively).

Measured dependencies of the diffracted light intensity on the light incidence angle at the LSAW excitation frequencies for all the IDTs used are shown in Fig. 5. For the LSAW wavelengths of 60, 50, 40, and 32 μm, the acousto-optic diffraction takes place in the configuration *a* of Fig. 3. For the wavelength of 120 μm, the diffraction corresponds to the configuration *d* of Fig. 3. Even though the LSAW frequency is the lowest for this IDT, the incidence angle is the highest.

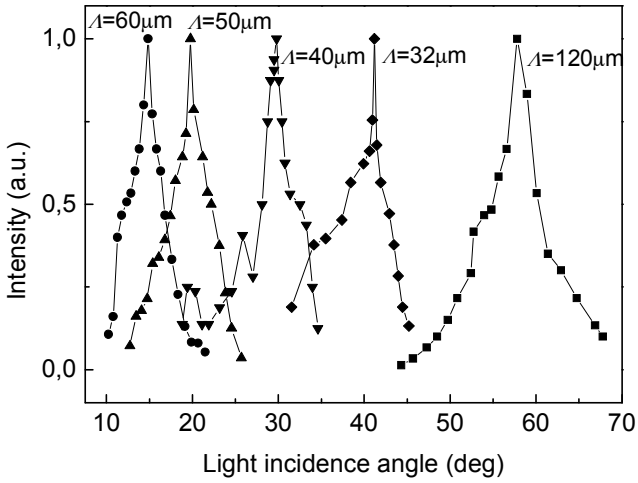

Fig. 5. Normalized intensities of diffracted light measured as function of light incidence angle.

The measured dependencies of the light incidence angle on the LSAW frequency for interaction configurations *a* and *d* of Fig. 3 are shown in Figs. 6*a* and 6*b*, respectively.

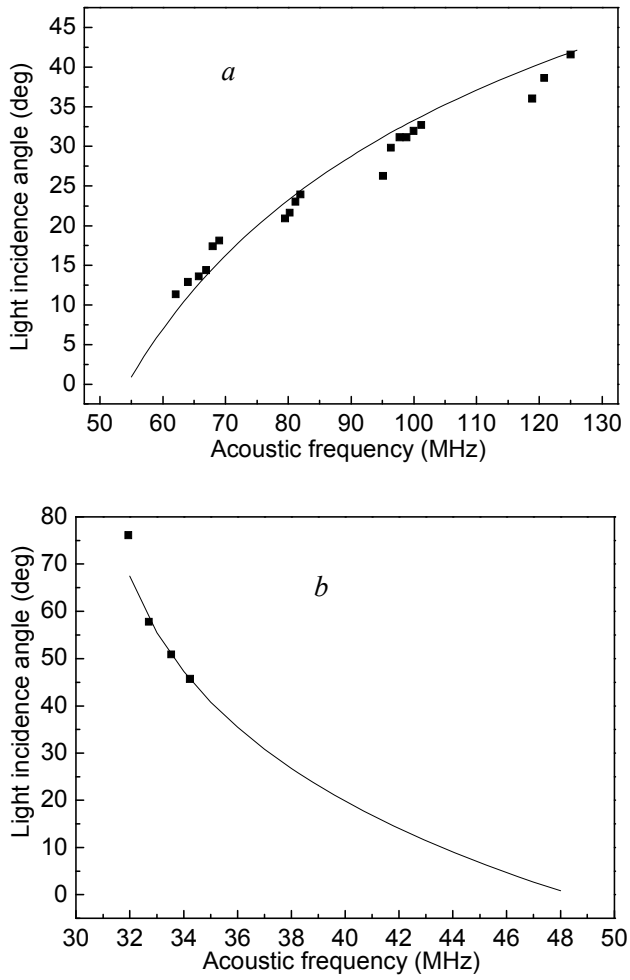

Fig. 6. Light incidence angle dependence on LSAW frequency. Dots, experiment; lines, calculation.

These dependencies exhibit opposite tendencies. The increase in the light incidence angle with growing acoustic frequency is observed for the case *a,* while the incidence angle decreases with increasing frequency in the case *d*. The dependencies of light incidence angle on acoustic frequency calculated from the Eqs. 3, 4 are also shown in Figs. 6*a* and 6*b* for comparison. In the calculations, we used the acoustic velocity V_B and the propagation angle α as fitting parameters. The best fit of measured and calculated curves is obtained with α=31^0, V_B =3530 m/s for results shown in Fig. 6*a*, and with α=35^0, V_B =3509 m/s for those of Fig. 6*b*. These values are in a reasonable agreement with the ones calculated from the phase matching condition (Eq. 1, see Table 1).

5 Conclusion

In conclusion, the light interaction with leaky surface acoustic wave radiation in YX-$LiTaO_3$ has been simulated and experimentally studied. In the case of anisotropic light diffraction, the dependencies of light incidence angle on the leaky surface acoustic wave frequency have been measured and calculated from the phase matching condition. The experimental curves are in good agreement with the calculated ones. The BAW propagation angle and corresponding velocity values were extracted from the best fit of measured and calculated results.

In the case of anisotropic acousto-optic diffraction in YX-$LiTaO_3$, the light incidence angles depend on acoustic frequency much more drastically, especially for the case *b* of Fig. 6, as compared to the interaction in ZX-$LiNbO_3$ [1]. Therefore, in YX-$LiTaO_3$, the higher precision of acoustic wave parameter evaluation can be achieved, and, on the other hand, the sensitivity of light control can be increased.

References

[1] R. Rimeika, D. Ciplys, P. Kazdailis, and M. S. Shur, “Anisotropic acousto-optic diffraction by leaky wave radiation in ZX-$LiNbO_3$,” Appl. Phys. Lett. 90, 181935 (1-3) (2007)

[2] P. Kazdailis, R. Rimeika, D. Ciplys, and M.S. Shur, “Light diffraction by IDT-radiated bulk acoustic waves in ZX-$LiNbO_3$”, Proc. 2007 IEEE International Ultrasonics Symposium, 2323-2326

[3] D. Royer and E. Dieulesaint, Elastic waves in solids, vol. 2. Berlin: Springer, 2000, p. 184

[4] K. Nakamura, N. Kazumi, H. Shimizu, “SH-type and Rayleigh-type surface waves on rotated Y-cut $LiTa0_3$”, Proc. 1977 IEEE International Ultrasonics Symposium, 819-822

[5] K. Hashimoto, M. Yamaguchi, S. Mineyoshi, O. Kawachi, M. Ueda, G. Endoh, “Optimum leaky-SAW cut of $LiTaO_3$ for minimised insertion loss devices”, Proc. 1997 IEEE International Ultrasonics Symposium, 245-254

[6] K. Yamanouchi, M. Takeuchi, “Applications for piezoelectric leaky surface waves”, Proc. 2007 IEEE International Ultrasonics Symposium, 11-18.

[7] D. Royer and E. Dieulesaint, Elastic waves in solids, vol. 1. Berlin: Springer, 2000, p. 148, 164